

## Two photon resonance enhanced multiphoton ionization spectroscopy and state assignments of the methyl radical

Jeffrey W. Hudgens@f@f, T. G. DiGiuseppe@f@f, and M. C. Lin

Citation: *J. Chem. Phys.* **79**, 571 (1983); doi: 10.1063/1.445857

View online: <http://dx.doi.org/10.1063/1.445857>

View Table of Contents: <http://jcp.aip.org/resource/1/JCPSA6/v79/i2>

Published by the [American Institute of Physics](#).

---

### Additional information on J. Chem. Phys.

Journal Homepage: <http://jcp.aip.org/>

Journal Information: [http://jcp.aip.org/about/about\\_the\\_journal](http://jcp.aip.org/about/about_the_journal)

Top downloads: [http://jcp.aip.org/features/most\\_downloaded](http://jcp.aip.org/features/most_downloaded)

Information for Authors: <http://jcp.aip.org/authors>

### ADVERTISEMENT



**ALL THE PHYSICS  
OUTSIDE OF  
YOUR JOURNALS.**

physics  
today

# Two photon resonance enhanced multiphoton ionization spectroscopy and state assignments of the methyl radical

Jeffrey W. Hudgens,<sup>a)</sup> T. G. DiGiuseppe,<sup>b)</sup> and M. C. Lin

Chemistry Division, Code 6185, Naval Research Laboratory, Washington, D.C. 20375

(Received 3 February 1983; accepted 8 April 1983)

A mass resolved multiphoton ionization spectroscopy study of  $\text{CH}_3$  and  $\text{CD}_3$  has revealed two new electronic Rydberg series in these radicals. Simultaneous absorption of two photons prepared the excited states. Absorption of a third photon from the excited state generated the parent ions of methyl radical ( $m/z$  15;  $\text{CH}_3^+$  and  $m/z$  18;  $\text{CD}_3^+$ ) which were detected in a quadrupole mass spectrometer. The  $np\ ^2A_2'$  Rydberg series was detected and identified by a rotational assignment of the  $3p\ ^2A_2''$  state of  $\text{CD}_3$  and by a polarization study of the  $np$  states. The quantum defect of this series was 0.6. The rotational constants determined for the ground and  $3p\ ^2A_2''$  excited states were  $B_0'' = 4.798\text{ cm}^{-1}$  and  $B_0' = 4.768\text{ cm}^{-1}$ . A vibrational analysis shows that both the symmetric stretch and out-of-plane bending mode are active in the  $3p\ ^2A_2''$  state. A second Rydberg series with a quantum defect of zero was detected and tentatively assigned to the  $nf\ ^2E'$  series.

## I. INTRODUCTION

The methyl radical is one of the most important molecular free radicals in chemical reactions. It plays an important role during the initial stages of hydrocarbon combustion and atmospheric chemistry. As one of the simplest hydrocarbons, it is a benchmark system for molecular orbital theory. Most of the understanding of methyl radical's electronic structure comes from vacuum ultraviolet spectra reported by Herzberg.<sup>1,2</sup> Resonance enhanced multiphoton ionization (REMPI) spectroscopy has also successfully detected these states.<sup>3-7</sup> Recently, we reported a series of new states observed as two photon resonances in  $\text{CH}_3$ .<sup>8</sup> In this report we present the two photon REMPI spectra of  $\text{CH}_3$  and  $\text{CD}_3$  and a description of the state symmetry assignments of these transitions.

In his pioneering spectroscopic studies on methyl radicals Herzberg observed three Rydberg series with the first member of each series at 216 (46 205  $\text{cm}^{-1}$ ), 149.7 (66 811  $\text{cm}^{-1}$ ), and 150.3 nm (66 536  $\text{cm}^{-1}$ ). Vibronic structure in  $\text{CH}_3$  and  $\text{CD}_3$  was also observed in these bands. The observed rotational structure in both isotopic species of methyl radical was not very sharp, but it was resolved sufficiently to allow analysis. A consistent interpretation of this vibronic and rotational structure required that methyl radicals be planar or deviate from planarity by less than  $10^\circ$ .

All evidence indicates that methyl radicals are planar. Interpretation of photoelectron spectra,<sup>8,9</sup> photoelectron detachment spectra,<sup>10</sup> electron spin resonance spectra,<sup>11,12</sup> and infrared spectra in matrix,<sup>13-16</sup> and gas phase<sup>17-19</sup> have required a planar structure within each technique's measurement limit. In a recent high resolution absorption study of  $\text{CH}_3$  radicals using a laser diode spectrometer, Yamada *et al.*<sup>18</sup> measured the  $\nu_2$  out-of-plane bending mode 1-0, 2-1, and 3-2 rovi-

bronic absorption bands with great precision and sensitivity. They noted that rotational levels;  $K=0, N=\text{odd}$  when  $\nu_2=\text{even}$  and  $K=0, N=\text{even}$  when  $\nu_2=\text{odd}$ ; are missing. These levels can only be absent when  $\text{CH}_3$  is of  $D_{3h}$  symmetry.

The vibrational spacings of the  $\nu_2$  mode also show a pronounced negative anharmonicity.<sup>14,17-19</sup> Yamada *et al.*<sup>18</sup> suggest that this negative anharmonicity may arise from a vibronically induced coupling between the ground and excited electronic states (e.g.,  $3s\ ^2A_1'$ ). In this view the barrier to inversion is zero and  $\text{CH}_3$  is planar.<sup>18,40</sup> The best fits of the infrared emission bands of the  $\nu_2=1-0$  to  $\nu_2=5-4$  transitions with model potential functions also support these conclusions.<sup>19</sup>

When sufficiently large basis sets are used, *ab initio* molecular orbital calculations also predict a planar  $D_{3h}$  methyl radical structure with no barrier to inversion.<sup>20-25</sup> In  $D_{3h}$  symmetry the ground state of methyl radical has the electron configuration

$$(1a_1')^2 (2a_1')^2 (2e')^4 (2a_2'')^1, \bar{X}\ ^2A_2''.$$

The ground state is of  $^2A_2''$  symmetry.

Figure 1 shows the higher energy molecular orbitals for a planar methyl radical and their correlation to the united atom, fluorine. All of these levels are Rydberg states and the state symmetry is the same as the molecular orbital symmetry. States that are allowed through one photon optical transitions by promotion of the  $2pa_2''$  electron are represented by solid lines. States that can be prepared only through simultaneous absorption of two or more photons are represented by dashed lines. In Fig. 1 arrows depict two photon transitions discussed in this paper. Table I lists the selection rules for single and multiphoton transitions from methyl radical's  $2p\ ^2A_2''$  ground state.

As a consequence of a planar structure, most states of the methyl radical cannot be observed by one photon spectroscopy: For example, transitions from the ground state to  $nde'$ ,  $npe'$ , and  $npa_2''$  states are one photon forbidden. One photon selection rules permit the transitions  $^2A_1' - ^2A_2''$  and  $^2E' - ^2A_2''$ . These rules

<sup>a)</sup> Author to whom correspondence should be addressed.

<sup>b)</sup> NRC/NRL Postdoctoral Research Associate. Present address: Geo-Centers, Inc., 320 Needham St., Newton Upper Falls, Massachusetts 02164.

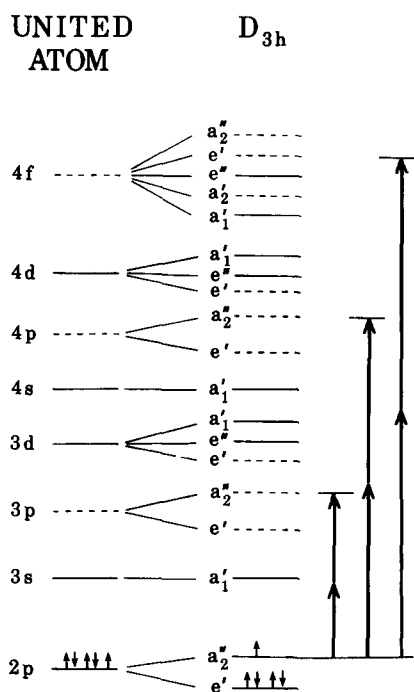


FIG. 1. The correlation diagram between united atom, fluorine, and the  $D_{3h}$  symmetry orbitals of methyl radical. States accessible by one photon absorption from the  $2p^2A_2''$  ground state are indicated by solid lines. Dashed lines indicate states accessible via multiphoton transitions. Arrows indicate the two photon transitions to states observed in this work.

predict that vacuum ultraviolet spectra should show only one  $ns-2p$  and two  $nd-2p$  one photon allowed Rydberg series. These Rydberg series were the only ones observed by Herzberg and provided important evidence for

methyl radical's planar structure.<sup>1,2</sup> Formally, two additional  $n\ell$  Rydberg series are one photon allowed, but these are expected to be weak<sup>2</sup> since they are one photon forbidden in the united atom representation.

Methyl radical also has one valence excited state formed by the promotion of a  $2pe'$  electron into the  $2pa_2''$  orbital to make the configuration (in  $D_{3h}$ ):

$$(1a_1')^2 (2a_1')^2 (1e')^3 (1a_2'')^2, \bar{A}^2E'$$

This state is also allowed only through multiphoton transitions. Molecular orbital calculations show that the lowest energy of this configuration is achieved with a pyramidal geometry.<sup>20</sup>

Another consequence of a  $D_{3h}$  structural symmetry is that only the  $\nu_1$  symmetric stretch vibrational mode may exhibit 1-0 or 0-1 vibronic structure in the electronic spectra. Other vibrational modes must occur as 2-0 or 0-2 bands.<sup>26</sup> In electronic spectra reported thus far, only the frequency of the out-of-plane bending mode  $\nu_2$  has been reported. In  $CH_3$  this mode's frequency greatly increases from  $\sim 606\text{ cm}^{-1}$  in the ground state<sup>18</sup> to  $\sim 1370\text{ cm}^{-1}$  in the Rydberg states.<sup>1-3,5,6</sup> In  $CD_3$  the  $\nu_2$  frequency changes from  $463^{15}$  to  $\sim 1060\text{ cm}^{-1}$ .<sup>2,5</sup>

In this paper we report a systematic REMPI study of the two photon spectroscopy of methyl radicals between laser wavelengths of 257 to 360 nm. Some of the  $CH_3$  two photon transitions have been reported previously.<sup>6</sup> In this paper we discuss the results in greater detail and present additional spectra. The symmetries of the two photon resonant Rydberg states are assigned from an analysis of the rotational structures of the bands. The two photon rotational selection rules have been calculated and the spectra are compared to com-

TABLE I. Optical selection rules for transitions from the vibrationless  $\tilde{X}^2A_2''$  state of methyl radical to singly excited states of other symmetries.<sup>a</sup>

Final vibronic ( $\psi_e\psi_v$ ) state symmetry species	Number of simultaneously absorbed identical photons		
	One photon	Two photons	Three photons
$^2A_1'$	$\Delta K = 0$ $K = 0; \Delta N = \pm 1$ $K \neq 0; \Delta N = 0, \pm 1$	f <sup>b</sup>	$\Delta K = 0$ $K = 0; \Delta N = \pm 1, \pm 3$ $K \neq 0; \Delta N = 0, \pm 1, \pm 2, \pm 3$
$^2A_1''$	f	$\Delta K = 0$ $K = 0; \Delta N = \pm 1$ $K \neq 0; \Delta N = 0, \pm 1, \pm 2$	$\Delta K = \pm 3$ $K'' = 0; \Delta N = \pm 1, \pm 3$ $K'' \neq 0; \Delta N = 0, \pm 1, \pm 2, \pm 3$
$^2A_2'$	f	f	$\Delta K = 0$ $K = 0; \Delta N = 0, \pm 2$ $K \neq 0; \Delta N = 0, \pm 1, \pm 2, \pm 3$
$^2A_2''$	f	$\Delta K = 0$ $K = 0; \Delta N = 0, \pm 2$ $K \neq 0; \Delta N = 0, \pm 1, \pm 2$	$\Delta K = \pm 3$ $K'' = 0; \Delta N = 0, \pm 2$ $K'' \neq 0; \Delta N = 0, \pm 1, \pm 2, \pm 3$
$E'$	f	$\Delta K = \Delta l = \pm 1$ $\Delta N = 0, \pm 1, \pm 2$	$\Delta K = 2(-\Delta l) = \pm 2$ $\Delta N = 0, \pm 1, \pm 2, \pm 3$
$E''$	$\Delta K = \Delta l = \pm 1$ $\Delta N = 0, \pm 1$	$\Delta K = 2(-\Delta l) = \pm 2$ $\Delta N = 0, \pm 1, \pm 2$	$\Delta K = \Delta l = \pm 1$ $\Delta N = 0, \pm 1, \pm 2, \pm 3$

<sup>a</sup>Hund's case (b) notation.

<sup>b</sup>f=forbidden process.

puter simulated rotational band contours. In our previous communication, we tentatively assigned the low lying Rydberg state as the  $^2E'$  state. However, the rotational analysis of our new data on  $CD_3$  indicates that this two photon resonant state is of  $^2A_2'$  symmetry.

## II. EXPERIMENTAL SECTION

The experimental apparatus has been described in detail<sup>3,5</sup> and only a brief description will be presented here. Methyl radicals were produced by pyrolysis in a resistively heated tantalum foil oven. Dimethyl sulfoxide (DMSO) and ditertiarybutyl peroxide (DTBP) were used as sources of  $CH_3$ . DMSO- $d_6$  (99.5%; Merck, Sharp, and Dohme; Canada) was pyrolyzed to produce  $CD_3$  radicals. The radicals produced in the oven passed through the hole in a thin plate and entered the ionization region of a differentially pumped quadrupole mass spectrometer. The linearly polarized output of a Nd:YAG pumped dye laser was focused into the ionization region. The total reagent pressure as measured with an ionization gauge in the quadrupole mass spectrometer was  $2 \times 10^{-6}$  Torr.  $CH_3$  band origins reported in this work were also observed in the effluent of a fast flow reactor that produced methyl radicals by the reaction of F atoms with  $CH_4$ .

The primary difference in these experiments from the three photon resonance experiments reported earlier was the wavelength region investigated for the two photon resonant transitions. The dye laser was pumped with either the second (at 532 nm) or third (at 355 nm) harmonic of the Nd:YAG laser. The dye laser output was frequency doubled with angle tuned KDP crystals. The optimum phase-matching angles were adjusted manually during each spectral scan. Presented in Table II are the Nd:YAG pump wavelength, laser dye, and frequency doubled wavelength region covered for each dye. The output of the doubling crystal passed through the appropriate glass filters to separate out the fundamental radiation.

The REMPI spectrum was obtained by measuring the mass 15 (mass 18 for  $CD_3$ ) ion signal as a function of dye laser wavelength. The spectra presented are not corrected for variations of the dye laser intensity. In the present work the relative laser intensity across any one band presented changes slowly enough that the band contour suffers little distortion. The wavelengths of the observed transition are reported as nanometers in air. The total energy of the resonant states are reported as  $cm^{-1}$  in vacuum. As can be seen in Table II, the wavelength region investigated in these experiments was 257 to 365 nm. Whenever possible, an effort was made to overlap the dye laser gain curves of several dyes for reasonable power levels at all wavelengths and for completeness of the spectral region investigated.

Polarization studies to determine the ion signal change as the laser light polarization changed from linear to circular were conducted for several of the stronger resonances. The optical components used for these studies consisted of a single escape Glan-Taylor polarizer ( $10^4:1$  extinction ratio), a double Fresnel rhomb, and a single Fresnel rhomb. The double

TABLE II. Laser dyes and pump wavelengths used to generate the laser wavelengths in this study.

Pump wavelength (nm)	Laser dye <sup>a</sup>	Spectral region (nm)
355	Coumarin 500	257–274
355	Coumarin 540A	269–278
355	Rhodamine 575	276–294
532	Rhodamine 560	282–288
532	Rhodamine 590	281–301
532	Rhodamine 610	301–318
532	Kiton red 620	290–320
532	DODC	318–332
532	Cresyl violet 670	317–336
532	Oxazine 720	327–337
532	Nile blue 690	342–365

<sup>a</sup>Methanol solutions.

Fresnel rhomb was mounted into a rotation stage and rotated in increments by a computer controlled stepper motor. First, the laser light was linearly polarized by the Glan-Taylor prism, then passed through the double Fresnel rhomb where its polarization plane was rotated  $2\theta$  where  $\theta$  is the angle of mechanical rotation of the double Fresnel rhomb relative to the position of no polarization rotation. Finally, the amount of polarization retardation was determined by the angle of the laser beam's polarization plane (after the  $2\theta$  rotation) relative to the optically active plane in the single Fresnel rhomb. With this apparatus laser beams of plane polarization could be generated at all wavelengths. The power aberration of beams of circular polarization was specified to be about 0.3% at 333 nm (the worst case).

## III. RESULTS AND ANALYSIS OF THE REMPI SPECTRA

### A. Vibronic bands observed in $CH_3$ and $CD_3$

The REMPI spectra of  $CH_3$  and  $CD_3$  between 325 and 336 nm are shown in Figs. 2 and 3, respectively. These signals are produced by the simultaneous absorption of two photons to prepare an excited Rydberg state in the radical. Absorption of one additional photon is necessary to ionize the radical. All spectra in this paper show the molecular ion currents  $m/z$  15 for  $CH_3$  and  $m/z$  18 for  $CD_3$  as a function of wavelength.

Tables III and IV list the observed radical resonances and their assignments for  $CH_3$  and  $CD_3$ , respectively. Table IV also notes the deuterium frequency shift. The band origins of electronic states are identified by their relatively small isotope shifts ( $\sim 86$   $cm^{-1}$ ). Vibronic levels of the excited states show much larger shifts. In  $CD_3$   $0_0^0$  levels are observed at 333.9, 286.3, 271.5, and 264.7 nm and in  $CH_3$  at 333.4 and 286.3 nm. These levels construct Rydberg series of  $n=3, 4, 5, 6$  for  $CD_3$  and  $n=3, 4$  for  $CH_3$ . The quantum defects of these series are 0.6. These quantum defects are consistent with those expected for the promotion of the ground state  $2pa_2''$  electron into an  $np$  Rydberg orbital. Below we show that this Rydberg orbital is the  $npa_2''$  orbital which causes the final state symmetry to be  $^2A_2''$ .

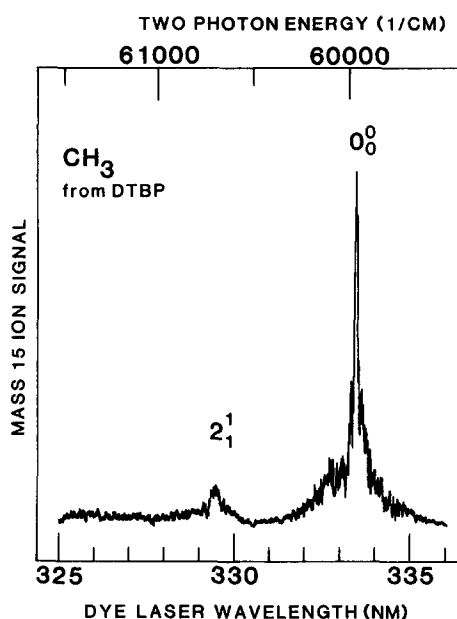


FIG. 2. The  $m/z$  15 ion signal observed for laser wavelengths between 325 and 336 nm showing the  $3p^2A_2''$  band origin of  $CH_3$  produced by the pyrolysis of the di-*t*-butyl peroxide.

A careful search was made for the  $n=5$  and  $n=6$  members of this Rydberg series in  $CH_3$  around 271 and 264.7 nm; however, no REMPI signal was detected. These experiments were done by measuring both the mass 15 ion signal and the total ion signal which would show any signal from dissociated molecular ions.

Only the  $3p^2A_2''$   $0_0^0$  band of  $CD_3$  at 333.9 nm showed well resolved S, R, Q, P, and O branches that allowed analysis. The  $CH_3$   $3p^2A_2''$   $0_0^0$  band showed no resolved rotational structure other than a prominent Q branch. All higher Rydberg states of the  $^2A_2''$  series showed spectra like those in Fig. 4. Figure 4 shows the REMPI spectra of the  $4p^2A_2''$  Rydberg states of both  $CH_3$  and  $CD_3$ . The only distinguishable feature in each compound's spectrum is a very strong, sharp Q branch.

Only the  $3p^2A_2''$  states of methyl radical show vibrational structure. Most of the vibrational activity occurs

TABLE III.  $CH_3$  Rydberg state transitions.

Transition		Wavelength (nm)	Two photon energy ( $cm^{-1}$ )
$3p^2A_2''$	$0_0^0$	333.4	59 972
	$2_1^1$	329.4	60 700
	$2_2^2$	319.1	62 660
	$1_0^1$	317.9	62 886
	$2_1^3$	315.6	63 355
	$2_0^4$	306.2	65 300
$4p^2A_2''$	$0_0^0$	286.3	69 837
$4f^2E'$	$0_0^0$	275.75	72 508
$5f^2E'$	$0_0^0$	266.7	74 961

TABLE IV.  $CD_3$  Rydberg state transitions.

Transition		Wavelength (nm)	Two photon energy ( $cm^{-1}$ )	Isotopic shift ( $cm^{-1}$ )
$3p^2A_2''$	$0_0^0$	333.9	59 886	-86
	$2_1^1$	330.7	60 466	-234
	$2_2^2$	327.8	60 995	
	$2_0^2$	322.75	61 955	-705
	$1_0^1$	322.9	61 917	-969
	$2_1^3$	320.0	62 473	-882
	$2_0^4$	312.7	63 941	-1359
$4p^2A_2''$	$0_0^0$	286.5	69 789	-48
$5p^2A_2''$	$0_0^0$	271.5	73 645	
$6p^2A_2''$	$0_0^0$	264.7	75 557	
$4f^2E'$	$0_0^0$	276.05	72 431	-77
$5f^2E'$	$0_0^0$	267.0	74 885	-76

in the  $\nu_2$  out-of-plane bending mode. Figures 2 and 3 show the  $\Delta\nu_2=0$  hot band transitions between the vibrationally excited ground states and their vibrationally excited  $3p^2A_2''$  states. As in the  $nd^2E''$  states of methyl radical, the  $2_1^1$  levels are observed to be shifted to the blue of the band origin.<sup>2,6</sup> This shift is a consequence of the  $\nu_2$  out-of-plane bending mode's large increase in frequency upon promotion into the excited state. For example, in  $CH_3$  the  $2_1^1$  vibronic resonance is blue shifted 728  $cm^{-1}$  from the  $0_0^0$  band origin as compared to the 746  $cm^{-1}$  blue shift observed in the one and three photon accessible  $^2E''$  state. In  $CD_3$  (Fig. 3) two  $\Delta\nu_2=0$  hot bands are observed;  $2_1^1$  at 329.4 nm and  $2_2^2$  at 327.8 nm.

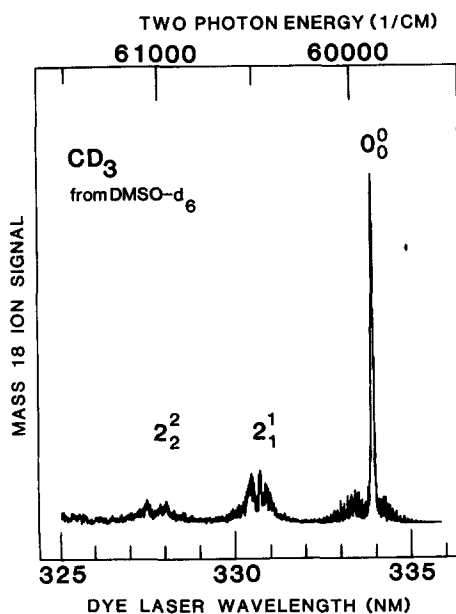


FIG. 3. The  $m/z$  18 ion signal observed for laser wavelengths between 325 and 336 nm showing the  $3p^2A_2''$  band origin of  $CD_3$  produced by the pyrolysis of dimethyl sulfoxide- $d_6$ .

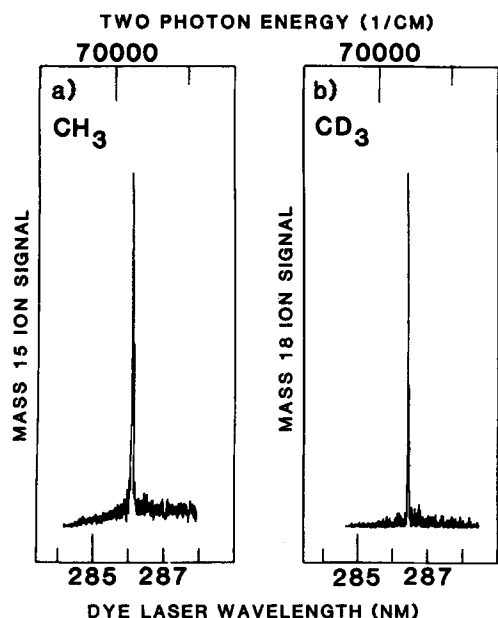


FIG. 4. The two photon resonance enhanced ionization signals observed from the  $4p\ ^2A_2''$  state of methyl radical. (a)  $m/z$  15.  $\text{CH}_3$  produced from the pyrolysis of DMSO, (b)  $m/z$  18.  $\text{CD}_3$  produced from the pyrolysis of  $\text{DMSO-}d_3$ .

Comparison of the vibronic structure between  $\text{CH}_3$  and  $\text{CD}_3$  in Fig. 5 reveals that the  $\nu_1$  symmetric stretch is also active. In  $\text{CH}_3$  a sharp band at 317.9 nm that does not fit into the  $\nu_2$  mode sequence is observed. Since  $\text{CD}_3$  shows no similar band near this wavelength, the 317.9 nm feature in  $\text{CH}_3$  cannot originate from a new electronic state. Instead, this band must originate from a second active vibrational mode. In  $\text{CD}_3$  the frequency of the isotopically shifted vibration is determined by noting that the band in the region of 322–323 nm in  $\text{CD}_3$  appears anomalous in both its intensity and structure. Its ion signal intensity was greater than the  $2_1^1$  or the adjacent  $2_1^3$  transition at the same laser power. The band features reproducible sharp peaks of diminishing intensity at 322.9 and 322.75 nm. The appearance suggested that this band in  $\text{CD}_3$  was either perturbed or a composite of two spectral transitions.

Figure 5 shows the expected isotopic shifts of the vibronic bands that arise by assigning the 317.9 nm transition in  $\text{CH}_3$  to the  $1_0^1$  band. The 317.9 nm peak is  $2914\text{ cm}^{-1}$  from the  $\text{CH}_3$  band origin. If this transition is assigned to the  $\nu_1'$  symmetric stretch, then the harmonic oscillator isotope shift,  $1\nu_1'/\sqrt{2}$ , will move this band to  $61954\text{ cm}^{-1}$  (322.74 nm) in  $\text{CD}_3$ . The harmonic oscillator deuterium isotope shift for the  $2_0^2$  band in  $\text{CH}_3$  is  $2\nu_2'/1.290$ . This predicts that the  $2_0^2$  band in  $\text{CD}_3$  lies at  $61977\text{ cm}^{-1}$  (322.61 nm)—or about  $23\text{ cm}^{-1}$  from the  $1_0^1$  band. These expected shifts are marked above the  $\text{CD}_3$  spectrum in Fig. 5 (lower trace). The larger isotope shift of the symmetric stretch compared to the out-of-plane bend causes the ordering of these levels to reverse. Because the  $2\nu_2'$  and  $1\nu_1'$  levels possess the same symmetry and reside at nearly the same energy, they undoubtedly interact via Fermi Resonance and only a high resolution spectrum of this band may resolve the relative mixture

TABLE V. Vibrational spacings of the  $3p\ ^2A_2''$  Rydberg state of methyl radicals.

Vibrational spacing	Energy ( $\text{cm}^{-1}$ )	
	$\text{CH}_3$	$\text{CD}_3$
$\nu_1' = 0 - \nu_1' = 1$	2914	2031 <sup>a</sup>
$\nu_2' = 0 - \nu_2' = 1$	1334	1032
$\nu_2' = 1 - \nu_2' = 2$	1350	1037 <sup>a</sup>
$\nu_2' = 2 - \nu_2' = 3$	1305	971 <sup>a</sup>
$\nu_2' = 3 - \nu_2' = 4$	1336	1015

<sup>a</sup>These levels are perturbed by Fermi Resonance and their spacings are approximate. See the text.

and identity of the various features in this band. However, for the construction of the spacings between vibrational levels we have assigned the sharp peaks in the 322 nm band according to the order expected from the isotope shifts. Thus, we assign the 322.9 nm peak as mostly  $1_0^1$  and the 322.75 nm peak as mostly  $2_0^2$ .

Table V lists the vibrational spacings within  $3p\ ^2A_2''$  band computed from the measurements listed in Tables III and IV. The energy spacing between the  $\nu_2' = 0$  and  $\nu_2' = 1$  levels are derived from the present data in combination with the ground state energy differences for the  $\nu_2$  mode measured by Yamada *et al.*<sup>18</sup> and Jacox<sup>13</sup> for  $\text{CH}_3$  ( $606\text{ cm}^{-1}$ ) and  $\text{CD}_3$  ( $463\text{ cm}^{-1}$ ), respectively.

#### B. Analysis of the rotational structure in the 333.9 nm band of $\text{CD}_3$

The Rydberg series quantum defect of 0.6 shows that this series probably originates from resonances with

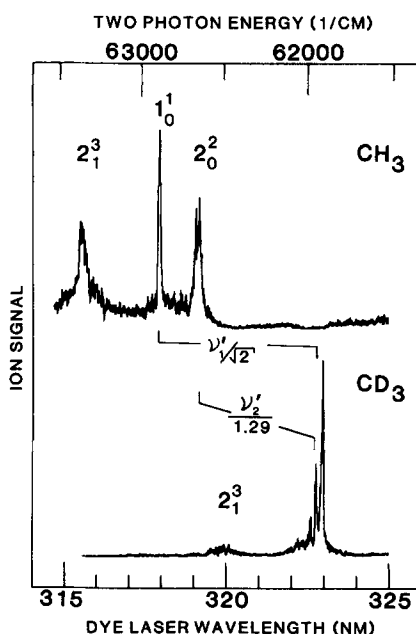


FIG. 5. Resonance enhanced ionization signals observed between 315 and 325 nm for  $\text{CH}_3$  (upper trace;  $m/z$  15) and  $\text{CD}_3$  (lower trace;  $m/z$  18). Correlation lines between the two spectra show the expected harmonic potential isotope shifts of the  $2_0^2$  and  $1_0^1$  vibronic transitions from  $\text{CH}_3$  to  $\text{CD}_3$ .

TABLE VI. Electronic Coriolis expectation values  $\zeta_e$  for Rydberg states centered upon the Carbon atom and evaluated from the hydrogenic basis set of the united atom.

Orbital symmetry <sup>a</sup>			
United atom	$D_{3h}$	$m_l$	$\zeta_e$
$ns$	$A_1'$	0	0
$np [z]$	$A_2''$	0	0
$np [x, y]$	$E'$	1	+1
$nd [2z^2 - x^2 - y^2]$	$A_1'$	0	0
$nd [xz, yz]$	$E''$	1	+1
$nd [x^2 - y^2, xy]$	$E'$	2	-2
$nf [z^3]$	$A_2''$	0	0
$nf [xz^2, yz^2]$	$E'$	1	+1
$nf [xyz, z(x^2 - y^2)]$	$E''$	2	-2
$nf [x(x^2 - 3y^2)]$	$A_1'$	3	0
$nf [y(3x^2 - y^2)]$	$A_2'$	3	0

<sup>a</sup>The phase conventions discussed in Ref. 30 for degenerate electronic states are adopted here.

$np$  orbitals.<sup>27</sup> These  $np$  Rydberg states have two possible state symmetries:  ${}^2E'$  and  ${}^2A_2''$ . Analysis of the rotational structure in the  $CD_3$   $0_0^0$  band at 333.9 nm provides an unambiguous symmetry assignment for the series.

The rotational energy levels of an oblate symmetric top that has unresolved spin-rotational interaction is

$$F_e(N, K) = T_e + B_0[N(N+1) - K^2] + D_N N^2(N+1)^2 + C_0(K - \zeta_e l)^2, \quad (1)$$

where  $B_0$  and  $C_0$  are the commonly used oblate symmetric top rotational constants ( $B_0 = 2C_0$  for a planar symmetric rotor) and  $D_N$  is the centrifugal stretching term. The term  $(K - \zeta_e l)$  is the magnitude of the nuclear top angular momentum,  $K$  is the signed quantum number of total angular momentum about the symmetry axis and varies between  $-N$  and  $+N$  including zero.<sup>28</sup>

The Coriolis term  $\zeta_e$  is the expectation value of the projection of the Rydberg electron's electronic angular momentum upon the symmetry axis<sup>28-31</sup>

$$\zeta_e = \langle \phi | L_z | \phi \rangle.$$

As a first approximation the wave function can be constructed from hydrogenic basis  $|n l m_l\rangle$  and evaluated only for the Rydberg electron. Table VI lists the Coriolis expectation values for the methyl radical Rydberg states evaluated in this manner. For pure  $3p {}^2E'$  Rydberg states centered upon the carbon atom,  $\zeta_e$  equals +1 ( $\zeta_e$  is usually observed to be around 0.9 rather than an integer value). Contributions from the hydrogen atoms can also change  $\zeta_e$ . We ignore vibrational Coriolis terms contributed by degenerate vibrational modes. Their effects should remain small as long as the vibrations remain inactive.<sup>36</sup>

The variable  $l$  serves only as a bookkeeping variable for the selection rules affecting the Coriolis term and

as such is a reflection of the transformation properties of the electronic wave function. For positive values of  $\zeta_e$ , " $l$ " takes on values of  $\pm 1$  when the electronic angular momentum is parallel (+1) or antiparallel (-1) to the projection  $K$  of total angular momentum vector upon the symmetry axis. For  ${}^2A_2''$  states both  $\zeta_e$  and  $l$  equal zero. Table I presents the changes in  $l$  for transitions from the electronic ground state.

Rotational line strength factors and two photon selection rules were derived in the context of Raman transitions by Placzek and Teller.<sup>32</sup> Mills has developed a simple and ingenious visual mnemonic which is useful for deriving any multiphoton selection rule.<sup>31</sup> The formula by Hougen<sup>33</sup> can also be directly applied to derive rules. Two photon rotational line strengths for two photon absorption by symmetric tops were more recently discussed by McClain<sup>34</sup> and tabulated by Chen and Yeung.<sup>35</sup> The two photon selection rules for  ${}^2A_2'' - {}^2A_2''$  transitions are those of a parallel band:

$$\text{For } K=0, \Delta N=0, \pm 2, \text{ and } \Delta K=0.$$

$$\text{For } K \neq 0, \Delta N=0, \pm 1, \pm 2, \text{ and } \Delta K=0.$$

Two photon selection rules for  ${}^2E' - {}^2A_2''$  are those for a perpendicular band:

$$\Delta N=0, \pm 1, \pm 2; \Delta K=+1, \Delta l=+1.$$

$$\Delta N=0, \pm 1, \pm 2; \Delta K=-1, \Delta l=-1.$$

Both types of bands have contributions from  $O, P, Q, R$ , and  $S$  branches. The  $\Delta K=0$  rule for  ${}^2A_2'' - {}^2A_2''$  transitions causes a very strong  $Q$  branch and simple  $O, P, R$ , and  $S$  branches when the rotational constants of the molecule do not change significantly. Each  $K$  component's contribution falls at nearly the same frequency for each particular quantum transition.

On the other hand the  ${}^2E' - {}^2A_2''$  bands are greatly affected by the  $\zeta_e$  and relative changes in the rotational constants. In prolate tops a transition with a  $\zeta_e = +1$  the Coriolis term can effectively compensate for the change in  $K$ . This compensation can cause "false" parallel bands.<sup>28</sup> In an oblate top this problem is not as severe and perpendicular bands are more easily recognized. In short, at the resolution of our experiments parallel bands can be assigned directly from the analysis of their rotational transitions. The more congested perpendicular bands can be analyzed by simulation.

Figure 6(a) shows the spectrum of the 333.9 nm band of  $CD_3$  expanded to show the rotational structure of the  $O, P, R$ , and  $S$  branches clearly. The very intense  $Q$  branch is not shown. The spectrum was generated using circularly polarized light. Individual  $N, K$  levels and their spin sublevels are not resolved. In fact, the widths of rotational features are broad and line positions can only be measured approximately. The width of these lines probably arises from unresolved frequency shifts contributed from each  $K$  member or perhaps from line broadening induced by predissociation, or by both. The spin-rotation splitting contribution to this broadening is probably insignificant. The broadening of these lines reduced the accuracy of our rotational constants enough that only the  $B_0$  values are significant.

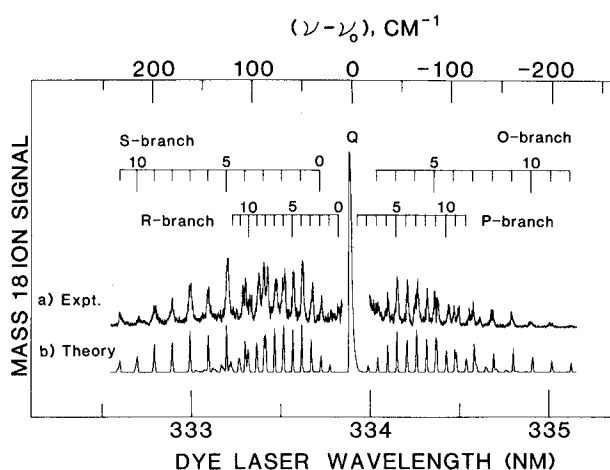


FIG. 6. Rotational spectrum and assignments of the O, P, R, and S branches of the  $3p^2A_2''$  band of  $CD_3$ . (a) The  $m/z$  18 resonance enhanced ionization signal produced with circularly polarized light. The very intense Q branch is not shown. (b) Computer generated simulation of rotational structure. See the text.

The spectrum is consistently analyzed by assigning the band as a  $3p^2A_2'' - \tilde{X}^2A_2'$  transition.

Table VII lists rotational constants determined from a least squares fit of the rotational line assignments listed in Table VIII. The assignment was based upon an  $^2A_2'' - ^2A_2'$  parallel transition. In Table VII the ground state rotational constants determined from the present measurements are compared with the ground state constants determined from the measurements by Herzberg. To do this, we have performed a least squares analysis upon Herzberg's published line positions<sup>2</sup> of the  $3s^2A_1' - \tilde{X}^2A_2''$  and  $3d^2A_1' - \tilde{X}^2A_2''$  bands of  $CD_3$ . The matrix used for this least squares analysis was constructed so that each band simultaneously contributed to the determination of the ground state rotational constants. The second set of entries in Table VII lists these constants and their standard deviations.

TABLE VII. Least squares rotational analysis of the observed Rydberg states of  $CD_3$ .

State	$T_e$ (cm <sup>-1</sup> ) <sup>a</sup>	$B_0$ (cm <sup>-1</sup> ) <sup>a</sup>	$D_N$ (cm <sup>-1</sup> ) <sup>a</sup>
This work's measurements only:			
$\tilde{X}^2A_2''$	0	4,798(29)	0,000 21(16)
$3p^2A_2''$	59 886.0(5)	4,768(24)	0,000 24(11)
Herzberg's measurements (Ref. 2) only:			
$\tilde{X}^2A_2''$	0	4,809(24)	0,000 56(29)
$3s^2A_1'$	46 627.9(7)	4,399(59)	0,000 87(42)
$3d^2A_1'$	66 726.1(7)	5,031(40)	0,000 38(22)
This work's measurements fitted together with Herzberg's measurements (Ref. 2):			
$\tilde{X}^2A_2''$	0	4,790(21)	0,000 19(12)
$3s^2A_1'$	46 627.8(5)	4,385(32)	0,000 41(21)
$3p^2A_2''$	59 886.3(5)	4,761(19)	0,000 23(10)
$3d^2A_1'$	66 725.2(5)	5,049(2)	0,000 22(10)

<sup>a</sup>Numbers in parentheses indicate the uncertainty of least significant figures.

TABLE VIII. Assignments of the rotational structure observed in the  $3p^2A_2'' - \tilde{X}^2A_2''$  band of  $CD_3$ .

$N'$	$N''$	$V_{obs}$ (cm <sup>-1</sup> )	$V_{obs} - V_{calc}$ (cm <sup>-1</sup> )
13	11	60 124.6	1.7
12	10	103.3	-2.3
11	9	88.6	0.6
10	8	71.2	1.1
9	7	53.0	0.9
8	6	34.3	0.5
7	5	16.1	0.6
6	4	59 998.0	1.0
11	10	991.9	-0.9
10	9	982.4	-2.0
5	3	978.1	-0.3
9	8	975.9	0.1
8	7	966.0	-1.1
4	2	958.6	-0.9
6	5	948.7	-0.4
5	4	940.9	0.9
4	3	930.5	-0.2
3	2	921.9	0.4
2	1	911.1	-1.0
3	4	854.6	0.3
1	3	845.1	0.1
5	6	834.8	0.1
2	4	824.5	-1.3
7	8	815.9	1.0
9	10	793.5	-1.4
11	12	775.4	0.8
5	7	769.4	1.6

The agreement between the ground state rotational constants computed from each data set agree very well. Rotational constants for the ground state of  $CD_3$  determined from Herzberg's data alone or from our data alone differ by less than either data set's standard deviation.

The third set of rotational constants in Table VII shows the results of a least squares fit of the present measurements and Herzberg's measurements together. To make this list the measurements of all three electronic transitions were incorporated into the same least squares matrix so that they all contributed to the fit of ground state rotational constants.

Table VIII lists the rotational line assignments and their deviations from the least squares computed line positions using the rotational constants determined from the present work's measurements. The rotational line positions marked above the spectra in Fig. 6(a) denote the  $K=0$  line positions of each rotational branch member as computed from the present work's rotational constants.

Figure 6(b) shows a computer generated simulation spectrum. The rotational constants of the present work only were used. Line strength factors from the work of Chen and Yeung<sup>35</sup> were adapted by substituting the quantum number  $N$  in place of  $J$  into their formulas. The use of circularly polarized light allowed us to sidestep the necessity of defining any value for Chen and Yeung's integral  $F$ . Integral  $F$  affects only the Q-branch intensity when the laser is linearly polarized. In principal, this integral is easily determined from a



TABLE IX. Polarization ratios of CH<sub>3</sub>.

Assignment	Wavelength (nm)	Ratio
3p <sup>2</sup> A <sub>2</sub> ''	0 <sub>0</sub> <sup>0</sup>	1.8
	2 <sub>1</sub> <sup>1</sup>	1.4
	2 <sub>0</sub> <sup>2</sup>	2.7
	1 <sub>0</sub> <sup>1</sup>	2.0
4p <sup>2</sup> A <sub>2</sub> ''	0 <sub>0</sub> <sup>0</sup>	2.3

polarization experiment when the rotational temperature is known.

To generate the CD<sub>3</sub> spectrum in Fig. 6(b), the rotational temperature was varied to achieve the best fit of the O, P, R, and S branch intensities with the experiment. The best rotational temperature was 300 K. This is not surprising since rotational relaxation rates are very rapid and the effusive flow of the CD<sub>3</sub> effluent from the pyrolysis oven has ample time at sufficient pressure to equilibrate with the background gas.

Of course, the simulation is not perfect. The lack of knowledge regarding the higher centrifugal distortion constants causes the frequency width of the higher *N* members of each rotational branch to be too narrow and their peak intensities to be too large. While the relative intensities of the  $\Delta N \neq 0$  branches agree well with experiment, the intensity of the simulated *Q* branch is nearly a factor of 3 too small.

### C. Results of polarization studies of CH<sub>3</sub> and CD<sub>3</sub>

The change in ion signal intensity as the laser beam's polarization changes from linear to circular provides a second way to determine the excited state's symmetry. The change in ion signal strength with polarization for resolved transitions is given by the ratio of the two photon absorption cross sections. In the case where both photons are absorbed from a laser beam tuned onto the *Q* branch of an <sup>2</sup>A<sub>2</sub>' - <sup>2</sup>A<sub>2</sub>'' band this polarization ratio is<sup>37</sup>:

$$\frac{I_1}{I_c} = \frac{2}{3} + \frac{10[N(N+1)(2N+3)(2N-1)]}{3[3K^2 - N(N+1)]^2} \left(\frac{F}{E}\right).$$

*F* and *E* are electronic-vibronic integrals listed by Chen and Yeung.<sup>35</sup> This polarization ratio will vary with temperature. For <sup>2</sup>A<sub>2</sub>' - <sup>2</sup>A<sub>2</sub>''  $\Delta N = \pm 1, \pm 2$  transitions and all <sup>2</sup>E' - <sup>2</sup>A<sub>2</sub>'' transitions, a polarization ratio of 2/3 is expected.

The principal result is that <sup>2</sup>E' - <sup>2</sup>A<sub>2</sub>'' transitions should show an *increase* in ion signal as the laser beam changes from linear to circular polarization. On the other hand an <sup>2</sup>A<sub>2</sub>' - <sup>2</sup>A<sub>2</sub>'' band's *Q* branch will show a *decrease* for the same polarization change.

The polarization ratios observed for the stronger resonances observed in CH<sub>3</sub> are listed in Table IX. For these measurements the laser's power frequency were held constant as the polarization was changed from linear to circular. In all measurements the ion signal

decreased as the laser beam's polarization changed from linear to circular. This behavior is the same as that expected for <sup>2</sup>A<sub>2</sub>' - <sup>2</sup>A<sub>2</sub>'' transitions. Unfortunately, the strength of any rotational branch transitions other than *Q* branches were too weak as compared to the background *m/z* 15 ion signal to render a useful polarization ratio measurement.

### D. Detection of a second Rydberg series

In the spectral region several nanometers to the red and blue of 276 nm CH<sub>3</sub> and CD<sub>3</sub> showed strong apparent continua; however, weak features were observed. Figures 7(a) and 8(a) show the ion signals in this spectral region for CH<sub>3</sub> and CD<sub>3</sub>, respectively. CH<sub>3</sub> shows a relatively sharp peak at 275.9 nm and broader absorption feature at 275.4 nm. The CD<sub>3</sub> spectrum shows a sharp peak at 276.1 nm and a broader feature at 275.9 nm. Both isotopic compounds show incompletely resolved fine structure. The fine structure in CH<sub>3</sub> is more varied in intensity and has wider frequency separations.

The deuterium isotope shift of the sharper peak of methyl radical 276 nm band is -55 cm<sup>-1</sup>. The broader peak has an isotope shift of -135 cm<sup>-1</sup>. These small shifts support the assignment of these features as band origins of a new state.

Figure 9 shows additional very weak bands in the spectra of CH<sub>3</sub> and in CD<sub>3</sub> at 266.8 and 267.1 nm. The figure shows the comparison spectra used to confirm that these bands originated with methyl radicals rather than from the radical's precursor. When the oven is at 1100 K, the radicals' resonances are seen. When the oven is cool and no radicals are generated, no reso-

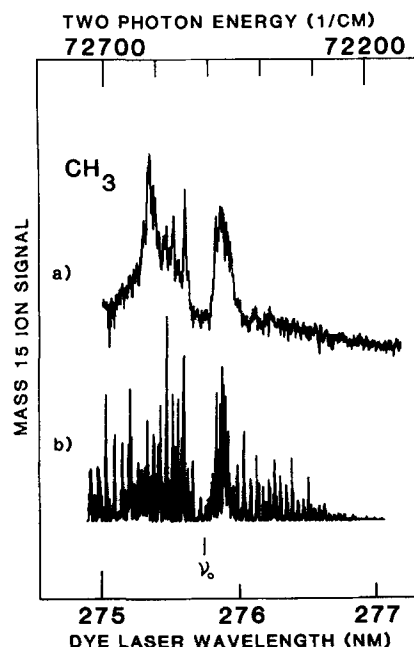


FIG. 7. Resonance enhanced ionization signals from CH<sub>3</sub> between 275 and 277 nm. (a) The observed *m/z* 15 REMPI spectrum; (b) the computer generated simulation of the spectrum. See the text.

nances are seen. The peaks show an isotope shift of  $-55\text{ cm}^{-1}$  and are assigned as new band origins. The 267 nm bands together with the 276 nm bands construct a new Rydberg series either of  $n=4,5$  with a quantum defect of zero or of  $n=5,6$  with a quantum defect of one. Either series converges upon the first ionization potential.

Experiments were conducted to detect any possible  $(n-1)$ th member (where  $n$  equals the assigned series value of the 276 nm band) of this Rydberg series. This band should occur at 297.6 nm and should be more intense than the 276 nm band. No resonances were detected. In fact in the spectral region from 287 to 320 nm neither  $\text{CH}_3$  nor  $\text{CD}_3$  show the slightest resonant ionization signal that can be assigned to any band origin.

The absence of any band origins around 295 nm in the present work does not confirm the assignment by Gedanken *et al.*<sup>38</sup> of a band at 294.9 nm to two photon resonances with methyl radicals. Their experiments were conducted in an ionization cell at 0.1 Torr pressure with no mass resolution capability. They based their assignment upon the observation that both  $\text{CH}_3\text{I}$  and tetramethyl tin displayed the same apparent two photon resonant band at this wavelength. They deduced that this resonance arose from methyl radical because it was believed that both compounds photolyze to produce large quantities of methyl radicals at this wavelength. A REMPI process following photolysis produced the ion signal.

Although the present results seem to place doubt upon the assignment by Gedanken *et al.*, their assignments should not be dismissed. The sensitivity of their apparatus cannot be determined because no values for

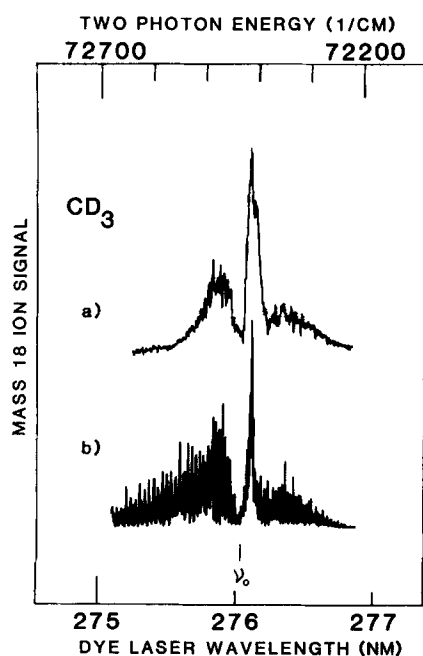


FIG. 8. Resonance enhanced ionization signals from  $\text{CD}_3$  between 275 and 277 nm. (a) The observed  $m/z$  18 REMPI spectrum; (b) the computer generated simulation of the spectrum. See the text.

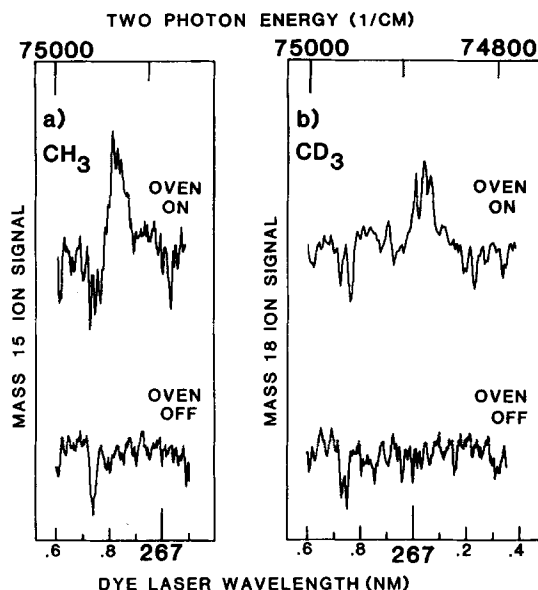


FIG. 9. Resonance enhanced ionization signals showing the  $5f$  Rydberg states of the methyl radical. (a) The sum of six laser scans viewing  $m/z$  15 ion signals from the effluent of the pyrolysis oven at 1100 (upper trace) and 300 K (lower trace); (b) a single laser scan viewing  $m/z$  18 ion signals from the effluent of the pyrolysis oven at 1100 (upper trace) and 300 K (lower trace).

the photolysis yield or product temperature are given. If every  $\text{CH}_3\text{I}$  molecule in the focal volume dissociates, the local concentration of  $\text{CH}_3$  radicals will be almost  $10^6$  times greater than in the present experiments. Thus, it is possible that their much higher radical concentration enables the detection of much weaker transitions than in our experiments. We conclude that if the resonance at 294.9 nm originates from the methyl radical, this band's two photon cross section is much weaker than the weakest bands reported in this present work (e.g., the 267 nm bands of  $\text{CH}_3$ ). The 294.9 nm band's weak intensity as well as its frequency also precludes any association of this tentative band with the present study's second Rydberg series.

#### IV. DISCUSSION

In brief, these are the observations:

(1) The  $np\ ^2A_2''$  Rydberg series has been observed in both  $\text{CD}_3$  and  $\text{CH}_3$  with a quantum defect of 0.6. The symmetry assignment is confirmed by an analysis of the  $3p\ ^2A_2'' - \bar{X}\ ^2A_2''$  rotational band. A polarization study also supports this assignment.

(2) The structure of the  $3p\ ^2A_2''$  state for the first four vibronic levels of the out-of-plane bending mode is presented. The frequency of the excited state symmetric stretch was also determined.

(3) Transitions to members of a second Rydberg series were detected.

These points will be discussed in order.

### A. Discussion of the $3p^2A_2''$ Rydberg states

The measured energy of the  $3p^2A_2''$  resonance of the present experiment may be compared to the molecular orbital calculations by Lengsfeld and Liu.<sup>42</sup> They have calculated the energies of the  $3p$  states using a double zeta with polarization basis set and configuration interaction obtained by doing all single and double excitations from one reference excitation. They compute that the  $3p^2A_2''$  state is  $57\,550\text{ cm}^{-1}$  (vert.) above the ground state. The present work's observed value is  $59\,972\text{ cm}^{-1}$ . Lengsfeld and Liu also calculate that the  $3p^2E'$  state is  $55\,630\text{ cm}^{-1}$  (vert.) above the ground state. McDiarmid<sup>20</sup> has calculated the vertical promotion energy to the  $3p^2E'$  state to be  $53\,152\text{ cm}^{-1}$  by means of a single configurational Hartree-Fock, optimized geometry calculation. Using the term values computed from each calculation's ionization potential, the estimated quantum defect of the  $np^2E'$  Rydberg series should be between 0.6–0.74. The  $3p^2E'$  Rydberg state's two photon resonance should lie between 330–345 nm.

The rotational analysis of the  $\text{CD}_3\ 3p^2A_2'' - \tilde{X}^2A_2''$  transition shows that the carbon-hydrogen bond lengthens only slightly upon promotion of the  $2pa_2''$  orbital electron into the  $3pa_2''$  Rydberg orbital. The bond lengths computed from the final entries of Table VII are  $1.079\text{ \AA}$  for the ground state and  $1.083\text{ \AA}$  for the  $3p^2A_2''$  state.

The basis for this small bond length change is seen in the fact that the  $2pa_2''$  orbital lies mostly above and below the carbon-hydrogen plane and is centered upon the carbon atom. Molecular orbital calculations of the ground state show that only about 4% of its electron density resides on the hydrogen atoms.<sup>25</sup> Thus, the  $2pa_2''$  orbital is essentially a nonbonding orbital. The  $3pa_2''$  orbital is also centered upon the carbon atom and maintains most of its electron density in the space above and below the nuclear plane with less electron density near the carbon where it can contribute to bonding. Thus, only a small bond length change is expected and observed upon the promotion of the  $2pa_2''$  mostly nonbonding electron into the even less bonding  $3pa_2''$  orbital.

The activity of the  $\nu_2$  mode has allowed observation of approximate positions of the first four vibrational levels of the out-of-plane bending vibration. As in the previously observed Rydberg states of  $\text{CH}_3$ , the  $\nu_2$  vibrational mode stiffens considerably from 606 to  $1330\text{ cm}^{-1}$ . Studies of the  $\nu_2$  vibrational mode in the  $\tilde{X}^2A_2''$  state in  $\text{CH}_3$  have shown that this mode has negative anharmonicity. However, in the  $3p^2A_2''$  state of  $\text{CH}_3$  this observed vibrational frequency is harmonic within the measurement of accuracy of each vibrational level (Table V). Yamada *et al.*<sup>18</sup> have accounted for the negative anharmonicity of the ground state  $\nu_2$  mode by an interaction with the excited  $3s^2A_1'$  state. Apparently, this interaction becomes much smaller for the  $3p^2A_2''$  state.

The active symmetric stretch mode in the  $3p^2A_2''$  state allows the first measurement of this mode's frequency for any state of methyl radical. Špirko and Bunker<sup>40</sup> have predicted a ground state frequency of  $2992.6\text{ cm}^{-1}$  for the  $1\nu_1'$  state in  $\text{CH}_3$ . They based their

prediction upon the fitting of several experimental data sets with a rigid inverter Hamiltonian. In the  $3p^2A_2''$  state of  $\text{CH}_3$  the observed  $1\nu_1'$  frequency is  $2914\text{ cm}^{-1}$ . Assuming that Špirko and Bunker's predicted ground state frequency is correct, the reduction of this frequency in the  $3p^2A_2''$  state is a measure of the small bonding contribution from the  $2pa_2''$  orbital's electron.

Špirko and Bunker<sup>40</sup> also predict a ground state  $2\nu_2''$  frequency in  $\text{CD}_3$  of  $966\text{ cm}^{-1}$ . Their prediction is supported by the present work's approximate measurement of  $2\nu_2'' = 960\text{ cm}^{-1}$  based upon the difference of the assigned  $2_2^2$  and  $2_0^2$  bands in the  $3p^2A_2''$  electronic state.

### B. Possible state assignments of the second Rydberg series

The second Rydberg series has several candidate electronic assignments. The not yet assigned  $nd^2E'$  and  $np^2E'$  Rydberg series present themselves as the first candidates for consideration. However, the present results do not mandate an obvious assignment to either of these Rydberg series. The problems of either assignment reside in the magnitudes of the quantum defects and in the fact that predicted bands are not detected.

If the bands observed at 276 and 267 nm are assigned to the  $4d^2E'$  and  $5d^2E'$  Rydberg states, then the experimental quantum defect of the series is zero. The lowest member of this Rydberg series, the  $3d^2E'$  state, should have its band at 297.6 nm. This band should be more intense than the band observed at 276 nm. No band was observed.

An assignment of these states to the  $nd^2E'$  series would also conflict with the expected ordering of the  $nd$  sublevels based upon crystal field splitting. This model predicts that the relative separation of the orbital sublevels is proportional to their  $-(m_l)^2$  values. In the  $\text{H}_3$  molecule the relative spacing of the  $3d$  and  $4d$  sublevels agree very well with this model.<sup>22,41</sup> In the methyl radical the one photon allowed  $nd^2A_1'$  ( $m_l=0$ ) and  $nd^2E''$  ( $m_l=1$ ) Rydberg series measured by Herzberg<sup>2</sup> fit the expected energy ordering. Based upon the assignments of these one photon allowed states, two photon resonances with members of the  $nd^2E'$  ( $m_l=2$ ) states of  $\text{CD}_3$  are predicted at 304.3, 278.4, and 267.8 nm. None of these predicted resonances fit with the observed.

If the observed bands are assigned to the  $5p^2E'$  and  $6p^2E'$  Rydberg states, then the experimental quantum defect is unity. A quantum defect of 1.0 is larger than generally accepted for an  $np$  Rydberg series.<sup>27,29</sup> The more intense  $3p^2E'$  and  $4p^2E'$  bands are expected at 384.9 and 297.6 nm. The predicted  $4p^2E'$  band was not detected. The present study did not span the spectral region of the hypothetical  $3p^2E'$  state.

In view of the problems with an assignment to either the  $nd^2E'$  or  $np^2E'$  Rydberg series, the  $nf$  Rydberg series should also be considered. The first members of each  $nf$  Rydberg series are the  $n=4$  members. The value of their quantum defects are essentially zero. In

methyl radical the first  $nf$  Rydberg two photon absorption bands are predicted to be at 276 nm. The following discussion shows that the band contour analysis is also consistent with an assignment of this series to the  $nf^2E'$  Rydberg series.

We have attempted to further resolve the state assignment issue by means of a band contour analysis. The approach was to simulate the rotational band contour of every possible candidate  $nf$ ,  $np$ , and  $nd$  Rydberg transition. As shown in Fig. 1, the united atom's  $4f$  level splits into components of symmetries  $^2E''$ ,  $^2E'$ ,  $^2A_1'$ ,  $^2A_1'$  and  $^2A_2'$ . States of  $^2A_1'$  and  $^2A_2'$  symmetry may be dismissed from consideration since they cannot be prepared by a two photon absorption process (Table I). The  $4f^2A_2''$  state is also eliminated since it will show the familiar parallel band structure. The features of this band cannot be accounted for by assuming that the resonances arise from a parallel band. Thus, the states considered in the band contour analysis were  $np^2E'$ ,  $nf^2E'$ ,  $nd^2E'$ , and  $nf^2E''$  Rydberg states.

The two photon allowed states of  $^2E'$  and  $^2E''$  symmetries will show perpendicular bands (Table I). The electronic states have differing sets of possible perpendicular bands shapes because their selection rules differ (Table I) and because they possess different electronic Coriolis coupling terms (Table VI). Only the  $nf^2E'$  and  $np^2E'$  states share the same selection rules and the same expected Coriolis coupling value. The other two possible candidate states  $nd^2E'$  and  $nf^2E''$  have unique parameters.

Recognition of the absorbing state's symmetry by its band shape also requires that the molecule conform to Hund's case (b) coupling. *A priori*, the energy separations of the  $4f$  symmetry states are expected to be small. When the states are close enough together, levels of angular momentum greater than zero will uncouple to produce a system conforming to Hund's case (d). Even when the state conforms to Hund's case (b), rotational levels can become split through  $\Lambda$  doubling which for a  $A-E$  two level interaction in case (b) is

$$E_{ea} = \frac{B_0^2 [N(N+1)]}{(E_e - E_a)}.$$

The interaction soon dominates and the system is represented by case (d). Herzberg, Hougen, and Watson<sup>41</sup> recently analyzed such a band in the  $H_3$  spectrum.

Whenever the molecular  $4f$  states are separated enough that the coupling is intermediate between Hund's cases (b) and (d), the  $CH_3$  bands will be affected more than the same  $CD_3$  band because uncoupling is dependent upon the magnitude of the rotational constant  $B'_0$ .

With these caveats in mind the results of the band contour calculations that best represent the 276 nm bands are shown in Figs. 7(b) and 8(b) for  $CH_3$  and  $CD_3$ , respectively, using the Hund's case (b) coupling scheme. This simulation uses the rotational selection rules and constants characteristic of either  $nf^2E' - \bar{X}^2A_2'$  or  $np^2E' - \bar{X}^2A_2'$  two photon transitions. Other excited state symmetries did not produce simulations that could be reconciled to either observed band. (In all of the

band contours we calculated, the rotational values chosen for the excited state were computed so that both isotopic species had the same internuclear distances.) The choices of Coriolis and rotational constants are not unique, but require that the excited state rotational value be larger than the ground state's. The Coriolis term could not be increased much above  $\zeta_e = 0.3$ .

The simulations fit the  $CD_3$  spectrum better than the  $CH_3$  spectrum. This is, in part, because no centrifugal terms were incorporated in making the diagrams that congest the spectrum and smooth its appearance. Unaccounted for uncoupling may also affect the observed spectrum. However, in both cases features near the band centers (band gaps as well as much of the prominent fine structure) lie at the same frequencies as in the actual spectra. Best fits of the width of the sharp and broad features as well as their contours and relative intensities occurred for the values  $B'_0 = 10.2 \pm 0.2$   $cm^{-1}$  and  $\zeta_e = 0.3$  for  $CH_3$  and  $B'_0 = 5.1 \pm 0.1$   $cm^{-1}$  and  $\zeta_e = 0.3$  for  $CD_3$ . In short, the band contour calculations rule out assignment of the 276 nm bands to resonances with  $nd^2E'$  and  $nf^2E''$  Rydberg states. On the basis of these calculations the series must arise from either the  $np^2E'$  or the  $nf^2E'$  Rydberg states.

Given the choice between these two Rydberg state assignments, the evidence supports an assignment to the  $nf^2E'$  Rydberg series much more than to the  $np^2E'$  series. Unlike for an  $np^2E'$  assignment, the  $nf^2E'$  state assignment accounts for all observed bands. No expected bands are missing. In addition, the experimental quantum defect of zero associated with an  $nf^2E'$  assignment is the proper value for this orbital type. The quantum defect of unity that results from an  $np^2E'$  assignment is too large. Thus, we tentatively assign these states at 276 and 267 nm to the  $4f^2E'$  and  $5f^2E'$  Rydberg states.

From the band contour results improved wavelengths for the band origins are assigned. These wavelengths are marked below the simulated spectra in Figs. 7 and 8. These assignments are also noted in Tables III and IV. From these assignments the isotopic shifts for these bands become  $-76$   $cm^{-1}$ . The values listed in the tables for the  $5f^2E'$  states are also the band origins extrapolated from the band contour results.

One surprising result from the calculations is that best value of the Coriolis term is low compared to the expected value of  $\zeta_e = 0.9$ .<sup>28-30</sup> In addition, the rotational constant in the excited state is larger than in the ground state which indicates that the C-H bond is shorter in the excited state. The effect of the excitation of the Rydberg orbital causes increased bonding. This increased bonding interaction of the Rydberg orbital with the hydrogens apparently reduces the Coriolis value.

In summary, the assignment of this second Rydberg series to two photon resonances with  $nf^2E'$  states seems to best fit the evidence. A theoretical effort at this point seems the most promising approach to confirm the identity of this series.

## ACKNOWLEDGMENT

The authors wish to express their appreciation to Dr. Jon T. Hougen of the National Bureau of Standards (Gaithersburg, MD) for his advice and discussions during the preparation of this work.

- <sup>1</sup>G. Herzberg and J. Shoosmith, *Can. J. Phys.* **34**, 523 (1956).
- <sup>2</sup>G. Herzberg, *Proc. R. Soc. London Ser. A* **262**, 291 (1961).
- <sup>3</sup>T. G. DiGiuseppe, J. W. Hudgens, and M. C. Lin, *Chem. Phys. Lett.* **82**, 267 (1981).
- <sup>4</sup>J. Danon, H. Zacharias, H. Rottke, and K. H. Welge, *J. Chem. Phys.* **76**, 2399 (1982).
- <sup>5</sup>T. G. DiGiuseppe, J. W. Hudgens, and M. C. Lin, *J. Phys. Chem.* **86**, 36 (1982).
- <sup>6</sup>T. G. DiGiuseppe, J. W. Hudgens, and M. C. Lin, *J. Chem. Phys.* **76**, 3338 (1982).
- <sup>7</sup>B. H. Rockney and E. R. Grant, *J. Chem. Phys.* **77**, 4257 (1982).
- <sup>8</sup>J. Dyke, N. Jonathan, E. Lee, and A. Morris, *J. Chem. Soc. Faraday Trans. 2* **72**, 1385 (1976).
- <sup>9</sup>T. Loenig, T. Balle, and J. Snell, *J. Am. Chem. Soc.* **97**, 662 (1975).
- <sup>10</sup>G. B. Ellison, P. C. Engelking, and W. C. Lineberger, *J. Am. Chem. Soc.* **100**, 2557 (1978).
- <sup>11</sup>M. Karplus, *J. Chem. Phys.* **30**, 15 (1959).
- <sup>12</sup>R. W. Fesenden, *J. Phys. Chem.* **71**, 74 (1967).
- <sup>13</sup>(a) D. E. Milligan and M. E. Jacox, *J. Chem. Phys.* **47**, 5146 (1967); (b) M. E. Jacox, *J. Mol. Spectrosc.* **66**, 272 (1977).
- <sup>14</sup>J. M. Riveros, *J. Chem. Phys.* **51**, 1269 (1969).
- <sup>15</sup>A. Snelson, *J. Phys. Chem.* **74**, 537 (1970).
- <sup>16</sup>J. Pacansky and J. Bargon, *J. Am. Chem. Soc.* **97**, 6896 (1975).
- <sup>17</sup>L. Y. Tan, A. M. Winer, and G. C. Pimentel, *J. Chem. Phys.* **57**, 4028 (1972).
- <sup>18</sup>C. Yamada, E. Hirota, and K. Kawaguchi, *J. Chem. Phys.* **75**, 5256 (1981).
- <sup>19</sup>H. W. Hermann and S. R. Leone, *J. Chem. Phys.* **76**, 4759 (1982).
- <sup>20</sup>R. McDiarmid, *Theor. Chim. Acta (Berlin)* **20**, 382 (1971).
- <sup>21</sup>G. T. Surratt and W. A. Goddard III, *Chem. Phys.* **23**, 39 (1977).
- <sup>22</sup>K. Morokuma, L. Pedersen, and M. Karplus, *J. Chem. Phys.* **48**, 4801 (1968).
- <sup>23</sup>P. Millie and G. Berthier, *Int. J. Quantum Chem. Symp.* **2**, 67, (1968).
- <sup>24</sup>Y. Ellinger, F. Pauzat, V. Barone, J. Donady, and R. Subra, *J. Chem. Phys.* **72**, 6390 (1980).
- <sup>25</sup>J. Pacansky, *J. Phys. Chem.* **86**, 485 (1982).
- <sup>26</sup>G. Herzberg and E. Teller, *J. Physik Chem. B* **21**, 410 (1933).
- <sup>27</sup>(a) M. B. Robin, *Higher Excited States of Polyatomic Molecules* (Academic, New York, 1975); (b) S. T. Manson, *Phys. Rev.* **182**, 97 (1969); (c) U. Fano, C. E. Theodosiou, and J. L. Dehmer, *Rev. Mod. Phys.* **48**, 49 (1976).
- <sup>28</sup>R. S. Mulliken and E. Teller, *Phys. Rev.* **61**, 283 (1942).
- <sup>29</sup>G. Herzberg, *Molecular Spectra and Molecular Structure* (Van Nostrand Reinholdt, New York, 1966), Vol. III.
- <sup>30</sup>H. F. King and K. Morokuma, *J. Chem. Phys.* **71**, 3213 (1979).
- <sup>31</sup>I. M. Mills, *Mol. Phys.* **7**, 549 (1964).
- <sup>32</sup>G. Placzek and E. Teller, *Z. Phys.* **81**, 209 (1933).
- <sup>33</sup>J. T. Hougen, *J. Chem. Phys.* **37**, 1433 (1962).
- <sup>34</sup>W. M. McClain and R. A. Harris, in *Excited States*, edited by E. C. Lim (Academic, New York, 1977), Vol. III.
- <sup>35</sup>K. Chen and E. S. Yeung, *J. Chem. Phys.* **69**, 43 (1978).
- <sup>36</sup>J. H. Van Vleck, *Rev. Mod. Phys.* **23**, 213 (1951).
- <sup>37</sup>This equation appears in Ref. 35, Eq. (15) with a typographical error which is corrected here.
- <sup>38</sup>A. Gedanken, M. B. Robin, and Y. Yafet, *J. Chem. Phys.* **76**, 4798 (1982).
- <sup>39</sup>Broadening mechanisms are not limited to predissociation. See, for example, E. H. Mies, *Phys. Rev. A* **20**, 1773 (1979).
- <sup>40</sup>V. Spirko and F. R. Bunker, *J. Mol. Spectrosc.* **95**, 381 (1982).
- <sup>41</sup>G. Herzberg, J. Hougen, and J. K. G. Watson, *Can. J. Phys.* **60**, 1261 (1982).
- <sup>42</sup>B. Lengsfeld and B. Liu (private communication).